JOURNAL OF APPLIED POLYMER SCIENCE VOL. 21, 2135–2155 (1977)

Melt-Spinning Dynamics and Rheological Properties of Nylon 6

VILAS G. BANKAR,* JOSEPH E. SPRUIELL, and JAMES L. WHITE,
Department of Chemical and Metallurgical Engineering, The University of Tennessee, Knoxville, Tennessee 37916

Synopsis

Basic studies of the melt-spinning dynamics and rheological properties of a nylon 6 polymer are described. The magnitude of the force components on the spinline has been analyzed with special reference to the drag and rheological forces. Spinline deformation has been investigated for spinning through ambient air and through an isothermal chamber. Both sets of experiments are interpreted using an elongational viscosity. Non-Newtonian viscosity was measured at 230°, 250°, and 270°C in a Weissenberg rheogoniometer and an Instron capillary rheometer. The principal normal stress difference was measured in the former instrument. The rheological properties are interpreted in terms of the theory of viscoelastic fluid behavior. The isothermal melt-spinning experiments were also interpreted in terms of the theory of viscoelastic fluids, and attempts were made to understand the spinning results in terms of basic rheological properties.

INTRODUCTION

The formation of fibers by the melt-spinning process is an industrial operation of great importance. One of the most important of melt-spun synthetic fibers on a worldwide basis is nylon 6, or polycaprolactam, $+(CH_2)_5—CO—NH+$.[1] The first rational synthesis of nylon 6 was due to Carothers and Berchet[2,3] in 1930, but moleular weights only of order 1000 were achieved. This was part of the research program which led to Carothers and Hill's[4] development of melt spinning synthetic polycondensate fibers. However, high molecular weight nylon 6 was not developed until the work of Schlack[5] in 1938, and commercialization as a melt spun synthetic fiber was due to the I. G. Farbenindustrie. In this paper, we will present a detailed study of the melt spinning of nylon 6, specifically the dynamics of the steady-state spinline under isothermal and nonisothermal conditions.

Many of the practical aspects of extrusion of nylons have been summarized by Bonner,[6] and Sbroli[1] describes melt-spinning technology. These authors point out the great chemical instability of nylon 6 brought on by heat and moisture and the need for precautions during processing. The extrudate swell and extrudate character of nylon 6 have been discussed by Ziabicki and Kedzierska[7]

* Present address: E. I. du Pont de Nemours and Co., Seaford, Delaware.

and Ishibashi.[8] Melt-spinning of nylon 6 has been studied by Ziabicki and Kedzierska,[7,9–12] Hamana, Matsui, and Kato,[13,14] and Ishibashi, Aoki, and Ishii.[15] None of these studies, however, contains basic rheological data or considers the melt-spinning process under isothermal conditions. The wet-spinning of nylon 6 fiber has been considered by Kiyotosukuri and his co-workers[16] and by Hancock, Spruiell, and White.[17]

Basic studies of the dyamics of the melt-spinning process were first reported by Ziabicki and Kedzierska[7,10,11] who made the first attempt at analysis of force components in a threadline and proposed an analysis using an elongational viscosity. This view was taken up and combined with a heat balance by Kase and Matsuo[18,19] to provide a complete model for spinline temperature and diameter. Hamana, Matsui, and Kato[14] later gave an improved model considering other spinline force components beyond the bobbin tension. Later researchers, notably Han and Lamonte,[20–22] attempted to improve the correlation of spinline data by using an elongational viscosity–elongation rate relationship. However, as first perhaps pointed out by White,[23] the polymer fluids spun into fibers are highly elastic; and, as shown by Bogue and White[24] and Acierno, Dalton, Rodriguez, and White[20] (see also Chen et al.[25]), viscoelastic constitutive equations need to be considered in spinline analyses. Other studies of the importance of viscoelastic behavior in spinline dynamics are those by Spearot and Metzner[26] and by Denn, Petrie, and Avenas.[27] The extrudate swell problem in melt spinning has been studied by White and Roman.[28] Critical reviews of the literature have been done by Ziabicki[29] and by White and Ide.[30]

Studies of the rheological properties of nylon 6 are few. Schaefgen and Flory[31] have studied the influence of molecular weight on the low shear-rate viscosity. A thorough investigation of the viscosity–shear rate behavior of polymers of this type as measured in a capillary rheometer has been reported by Pezzin and Gechele.[32] A recent literature survey of melt viscosity behavior of nylons is given by Kohan.[33] Unpublished studies of the viscosity of molten nylon 6 have also been carried out in various industrial laboratories. Such data have, for example, been supplied to us by Kotliar.[34] We are aware of no published research on viscoelastic properties, though limited studies of this type seem to have taken place in industrial laboratories.

The research presented in this paper involves a careful study of the rheological properties of a nylon 6 melt and the dynamics and deformation mechanics of the melt spinning of a fiber from this polymer. In a related study, the authors have considered structure development in nylon 6 during the melt-spinning process.[35] This paper is a continuation of studies at the University of Tennessee on the melt-spinning process.[20,25,28,30,35–41]

EXPERIMENTAL

Materials

Nylon 6 chips were obtained from the American Enka Company (Lowland, Tennessee). Before being characterized or spun into fiber, the nylon 6 was dried in a vacuum oven at 110°C for 16 hr followed by 4 hr of cooling. The moisture content was brought down to 0.03–0.04% as measured in a MEECO Electrolytic Moisture Analyzer. The intrinsic viscosity of the dried polymer measured in 85% formic acid/water at 20°C was 1.22. According to the American Enka

Laboratories the polymer had a number-average molecular weight of 22,500 and a ratio of weight-average to number-average molecular weight of 2.08.

No account was taken of the influence of moisture in degrading the polymer to different extents due to varying chemical equilibrium and rate constants at the various temperatures investigated in the rheological experiments.

Melt Spinning

The fibers were melt spun from a Fourné Associates screw extruder with a 1.3-cm diameter screw. At one end, it is connected to a 7-l. N_2-purged hopper through which dry nylon pellets were fed. At the other end of the extruder, it is metered through a gear pump, a 325-mesh screen, and a distributer plate to a capillary of diameter 0.0762 cm and length/diameter ratio of 5. The extrusion rate was 2.5 cm^3/min. The melt temperature, measured before the melt enters the spinneret block, was 262°C.

The fiber was taken up in our experiments with two different Leesona winders. It was taken up at speeds from 100 to 550 meters per min using a Leesona 955 winder. For take-up velocities $v(L)$ from 500 to 2400 meters/min, a Leesona 959 SCR winder was used. This is equivalent to draw down ratios $v(L)/v(0)$ of up to 100 on the 955 winder and 435 on the 959 winder. Here, $v(0)$ is the extrusion velocity. The fiber take-up velocity was maintained at a chosen value by passing the fiber around a feed roll rotated by a dc motor and controlled by a motor controller. After being wound at least four turns around the feed roll and an idler roll, it was passed to the winder and wound at constant tension. The apparatus is shown schematically in Figure 1.

The extruder was attached to a large column and positioned so that filaments could be passed through a rotating-anode x-ray generator. The table top of the generator served as a measuring stage and provided support for accessory devices for diameter and temperature measurements. The equipment also allowed studies of structure development during melt spinning, including on-line x-ray patterns and birefringence measurements. The results of these investigations will be reported in a subsequent paper.[35]

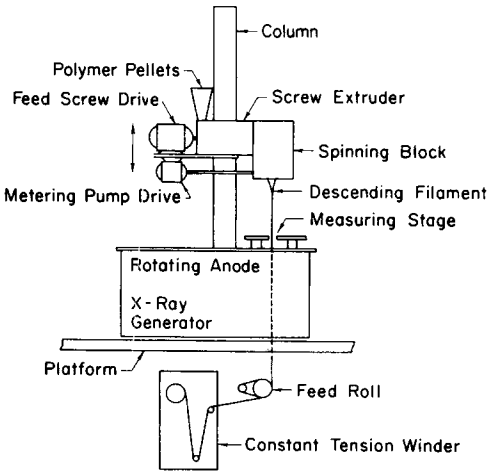

Fig. 1. Melt-spinning apparatus.

Spinline diameters were measured by photographing the running fiber using a Nikon 35-mm camera. The negatives were projected on a screen and the diameters determined. Surface temperatures of the running filament were measured using a Hastings Raydist matching temperature contact thermocouple and a null balance technique involving a sensitive potentiometer. Spinline tensions were measured using a Rothschild tensiometer with a 10-g measuring head.

In some experiments, an isothermal chamber was placed below the spinneret. This was the same chamber used in our earlier papers.[24,29] The chamber was 7 in. long and had two 6-in.-long, ¾-in.-wide windows placed so that the filament profile could be viewed. The chamber was maintained at 270° ± 2°C, and photographs of the filament diameter were taken through the windows.

Rheological Measurements

The shear viscosity of the nylon 6 melt was determined at 230°, 250°, and 270°C using both an Instron capillary rheometer and a Weissenberg rheogoniometer. The viscosity was measured in the capillary rheometer using three dies of diameter D of 0.02(3) in. and length/diameter (L/D) ratios of 9.4, 32.8, and 55.7. Specifically, the shear stress σ_{12} was determined at the capillary wall using the force balance

$$p_T = 4(\sigma_{12})_w \frac{L}{D} + \Delta p_e \tag{1}$$

where p_T is the total pressure, Δp_e is the end pressure loss, and the subscript w refers to evaluation of the capillary wall. The shear rate of this position was determined using Weissenberg's relationship[42,43]

$$\dot{\gamma}_w = \left(\frac{3n' + 1}{4n'}\right) \frac{32Q}{\pi D^3} \tag{2}$$

where

$$n' = \frac{d \log (\sigma_{12})_w}{d \log (32Q/\pi D^3)}$$

Data were obtained in the range of 50 to 1000 sec^{-1}.

The viscosity was measured in the rheogoniometer by determining the torque of a specific rotation rate in a known geometry. The samples were prepared by extrusion from the capillary rheometer barrel (without the presence of the die) followed by sectioning and drying as described above. A dry N_2 atmosphere was maintained in the rheogoniometer. The shear stress and shear rate were determined using Weissenberg's expressions[43,44]

$$\sigma_{12} = \frac{3M}{2\pi R^3} \tag{3}$$

$$\dot{\gamma} = \frac{\Omega}{\alpha} \tag{4}$$

where M is the torque, R is the cone radius, Ω is the angular velocity, and α is the angle between the cone and the plate. A cone of radius 2.5 cm and angle of 3°56′ was used.

The principal normal stress difference N_1 ($=\sigma_{11} - \sigma_{22}$) was also measured in the rheogoniometer using vertical thrust (force) F measurements. Specifically, we used the expression[43,44]

$$N_1 = \frac{2F}{\pi R^2} \tag{5}$$

It was observed that at the end of the experiments, part of the polymer had changed its appearance from white to dark brown or black. This was observed mainly at the outer edge of the polymer sample. The polymer within the gap remained almost the same in appearance as the original sample. It was apparent that some of the polymer was degrading or changing chemically during the experiment. In order to check this, the viscosity was measured on the same sample first with increasing shear rate and then with decreasing shear rate. No detectable change was observed when measurements were made at 230° and 250°C. A slight decrease was observed at 270°C.

Data were obtained in the range of 0.1 to 20 sec^{-1}. At shear rates greater than 5 sec^{-1}, the melt in the outer regions of the cone–plate apparatus balled up and exuded out of the gap.

NONISOTHERMAL MELT SPINNING

Kinematics and Temperature Profile

In Figure 2, we plot the measured variation in fiber diameter d as a function of position in the spinline with take-up velocity $v(L)$ as a running parameter. As take-up velocity increases, fiber diameter decreases more rapidly. In Figure 3, the variation of spinline temperature T as a function of position is plotted for the same set of take-up velocities. Increasing take-up velocity increases the rate of cooling of the fiber.

The variation of local spinline velocity with position may be computed using the expression

$$G = \rho(x) \frac{\pi d^2(x)}{4} v(x) = \text{constant} \tag{6}$$

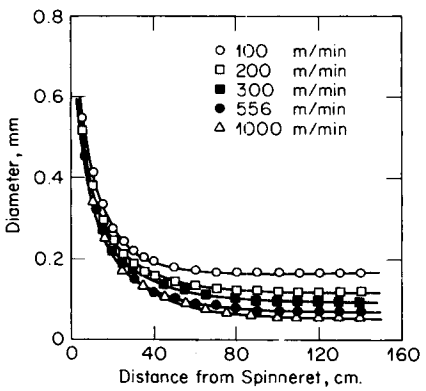

Fig. 2. Spinline diameter d as a function of position at various take-up velocities.

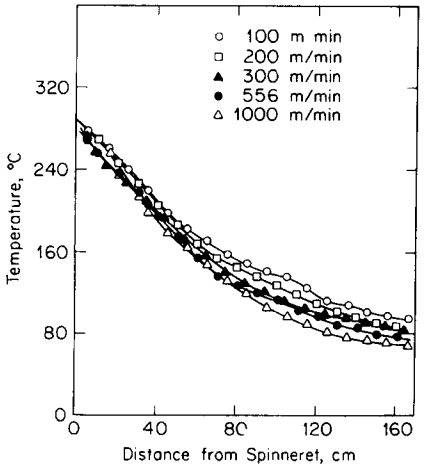

Fig. 3. Spinline temperature T as a function of position for various take-up velocities.

where G is the mass flow rate and ρ is the density. As $d(x)$ and G are known, $v(x)$ can be computed if $\rho(x)$ can be determined. Inoue[45] has given the variation of equilibrium density with temperature as shown in Figure 4. Inoue's data include an abrupt transition corresponding to crystallization. As shown by Bankar, Spruiell, and White,[35] nylon 6 does not crystallize in the spinline. This makes the use of the lower-temperature (crystalline) portions of Inoue's data inappropriate. We have used (see Fig. 4) extrapolated amorphous densities for computing low-temperature $v(x)$. In Figure 5, we plot the calculated spinline velocity as a function of position. Spinline velocity increases with distance from the spinneret and with take-up velocity. The velocity gradients dv/dx exhibit maxima.

Spinline Forces

The variation of spinline take-up force F_L and spinline stress $\sigma \equiv [F_L/(\pi d^2/4)]$ with take-up velocity is shown in Figure 6. Both increase with take-up velocity.

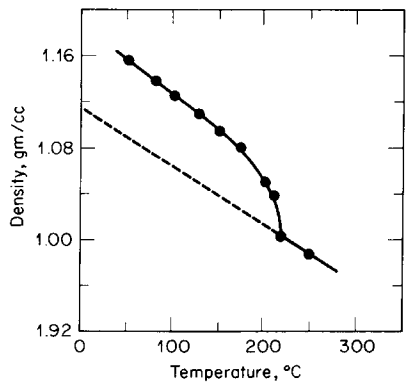

Fig. 4. Density–temperature relationship for nylon 6 as a function of temperature after Inoue.[45] Extrapolated amorphous density is shown with dashed line.

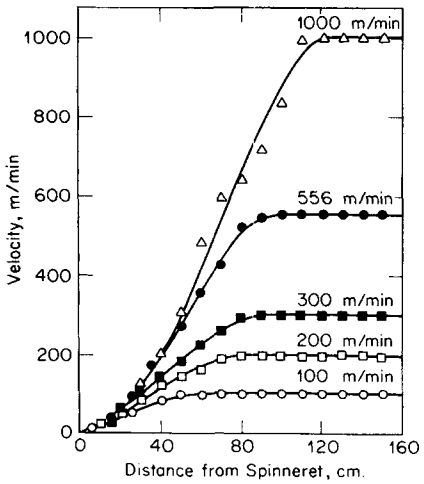

Fig. 5. Local spinline velocity as a function of position with different take-up velocities.

The actual force, F_{rheo}, that acts to deform the descending fiber is not equal to F_L. As shown by Ziabicki,[11,29] the force on a moving threadline includes gravitational force F_{grav}, frictional drag F_{drag}, and inertial force F_{inertia}. Thus, to obtain F_{rheo}, we must construct a force balance between position x and the take-up roll. This is

$$F_{\text{rheo}} = F_L + F_{\text{grav}} - F_{\text{drag}} - F_{\text{inertia}} \tag{7}$$

where

$$F_{\text{grav}} = \int_x^L \rho g \frac{\pi d^2(x)}{4} dx \tag{8a}$$

$$F_{\text{drag}} = \int_x^L \sigma_f \pi d(x)\, dx \tag{8b}$$

$$F_{\text{inert}} = G[v(L) - v(x)]. \tag{8c}$$

Here, σ_f is the shearing stress on the surface of the fiber.

Calculation of F_{grav} and F_{inertia} are straightforward using the available experimental data. F_{drag} is a problem because we must know σ_f. There have been

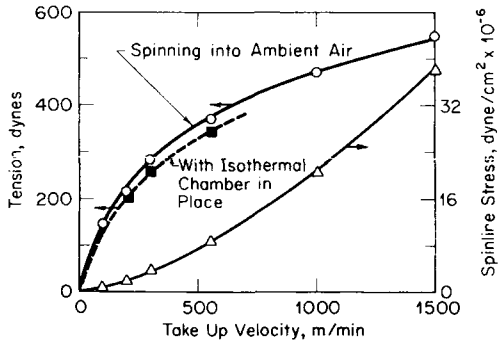

Fig. 6. Take-up force and tensile stress as a function of take-up velocity.

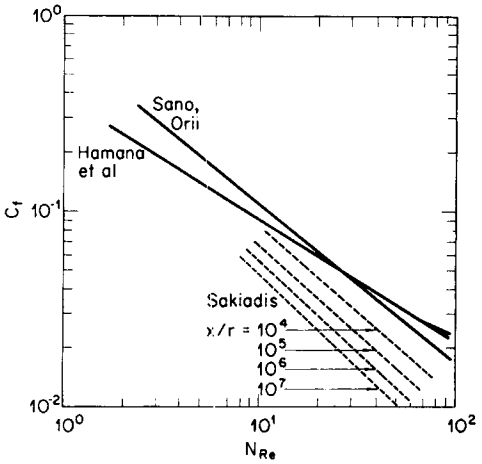

Fig. 7. Friction factor–Reynolds number data on fiber spinlines from the literature.

several theoretical and experimental studies of this problem.[4,29,46–48] Generally, we write

$$\sigma_f = c_f \frac{\rho v^2}{2} \tag{9}$$

where c_f is a friction factor which depends on fiber Reynolds number $N_{\mathrm{Re}} = dv\rho_a/\eta_a$ (where the subscript a refers to air) and the fiber radius of curvature. The different c_f–N_{Re} relationships in the literature are plotted in Figure 7. Generally, the experimental correlations of Hamana, Matsui, and Kato[14] and Sano and Orii[47] are similar, but the c_f for the theory of Sakiadis[46] is rather lower. Here, we have used the laminar flow boundary layer analysis of this author.

In Figures 8(a) and 8(b), we show computed values of F_{grav}, F_{drag}, F_{inertia}, and F_{rheo} as a function of spinline position for take-up velocities of 100 m/min and 1000 m/min. Solid lines show the values of F_{drag} in terms of Sakiadis theory, and dashed lines show values for Hamana, Matsui, and Kato's experimental c_f. At low take-up velocities and large filament diameters, F_{grav} is important. At intermediate take-up velocities, F_{grav} and F_{drag} tend to cancel out, while at high take-up velocities, F_{drag} and F_{inertia} become increasingly important. At low take-up velocities, F_{rheo} decreases along the spinline, while at high take-up velocities it increases.

In plots of these forces and data tabulation by earlier researchers,[14,25,33,34] usually low take-up velocities are considered and only Sakiadis and other theoretical boundary layer measurements of frictional drag are utilized. These papers may underestimate the effect of frictional drag.

Interpretation of Rheological Response in Terms of Elongational Viscosity

Basically, we are investigating from a rheological point of view a transient nonlinear, nonisothermal problem. This is beyond our current capability of analysis. (For a possible approach, see the discussion of Abbott and White.[36])

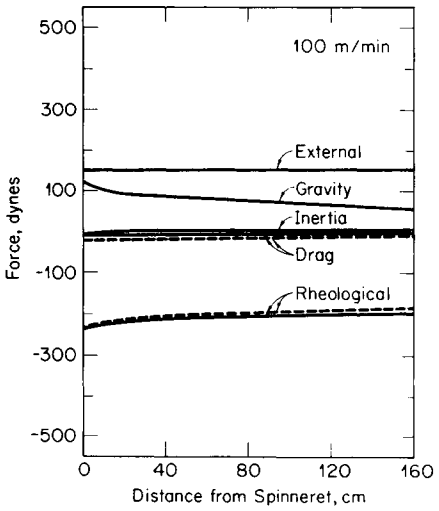

(a)

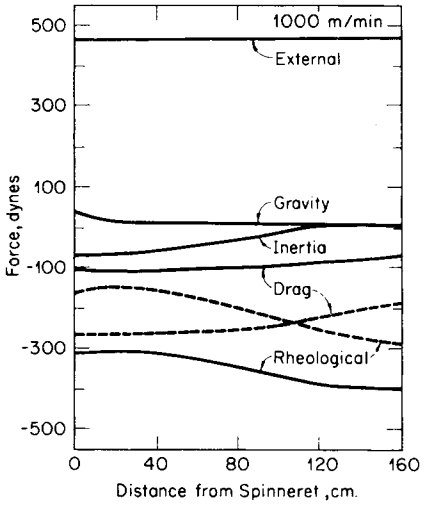

(b)

Fig. 8. Spinline forces F_{grav}, F_{drag}, $F_{inertia}$, and F_{rheo} as a function of spinline position: (a) 100 m/min; (b) 1000 m/min.

We have chosen here to use the simple traditional approach of Kase and Matsuo[18] and later researchers of representing the rheological response in terms of an elongational viscosity defined by

$$\chi(T) = \frac{F_{rheo}/(\pi d^2/4)}{dv/dx} \tag{10}$$

where dv/dx is the axial velocity gradient. This varies with temperature according to its spinline position.

As found in the previous section, F_{rheo} is strongly influenced by the expression used for F_{drag}. We plot our $\chi(T)$ data in Figure 9, where we have used the ex-

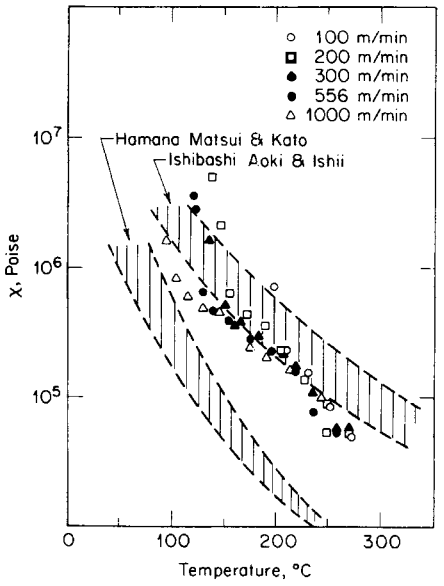

Fig. 9. $\chi(T)$ Function for nylon 6 using the Sakiadis expression for F_{drag}.

pression of Sakiadis for F_{drag}, and in Figure 10, where we have applied Hamana, Matsui, and Kato's counterpart. There is greater scatter in the data of lower temperatures than higher temperatures in both plots. There is, however, a much greater separation of experimental data from runs with varying take-up velocity when Hamana et al.'s expression is used.

In earlier experimental studies, Hamana, Matsui, and Kato[14] and Ishibashi, Aoki, and Ishii[15] have determined $\chi(T)$ in melt spinning of nylon 6. Their ex-

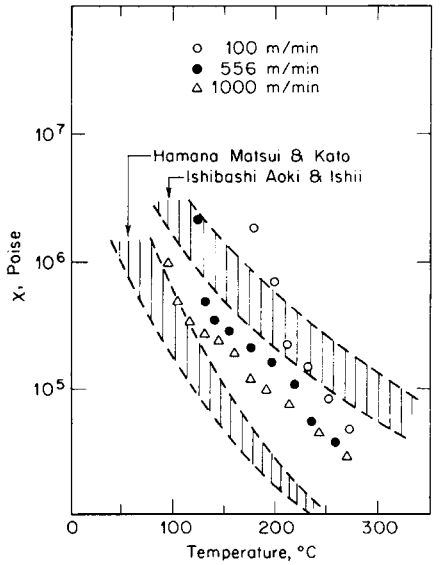

Fig. 10. $\chi(T)$ Function for nylon 6 using Hamana, Matsui, and Kato's expression for F_{drag}.

perimental results are also summarized in Figures 9 and 10. The $\chi(T)$ values of Ishibashi et al. are slightly higher than our results, and those of Hamana et al. are lower. This difference appears to be due to differences in molecular weights of the nylon 6 used in these studies. Ishibashi et al. report M_n for their nylon 6 (measured after extrusion) to be 19,000. Hamana et al. report that the viscosity-average molecular weight of their polymer was 16,000. If their $[\eta]$-versus-molecular weight relationship was based on narrow fractions, then M_η/M_n is approximately 1.8 and their $M_n < 10{,}000$. The M_n for our own polymer (measured on the dried chips) is of order 23,000.

The maximum in dv/dx can be explained by noting that eq. (10) may be rearranged to give

$$\frac{dv}{dx} = \frac{4F_{\text{rheo}}}{\pi} \cdot \frac{1}{d^2(x)\,\chi(x)} \tag{11}$$

The value of dv/dx is determined by the relative variation of χ and d. The values of $d(x)$ decrease approximately exponentially, so that at first, decreases in $d(x)$ outweigh increases in $\chi(x)$ caused by the decreasing temperature. However, further movement down the spinline results in a flattening of $d(x)$; but continued increases in $\chi(x)$ which eventually becomes very large, cause dv/dx to go to zero.

ISOTHERMAL MELT SPINNING

Kinematics and Spinline Tension

In Figure 11, we plot the typical diameter profiles obtained for the nylon 6 fiber in the isothermal experiments. Figure 12 shows local velocity as a function of spinline position.

The variation of spinline tension with take-up velocity is shown for the isothermal melt spinning case in Figure 6 and is compared with the nonisothermal tension. Generally, the tension is lower when the isothermal chamber is in position.

Preliminary Interpretation

The simplest rheological interpretation of the experimental data is to use the elongational viscosity χ of eq. (10) but allow it to vary with elongation rate dv/dx

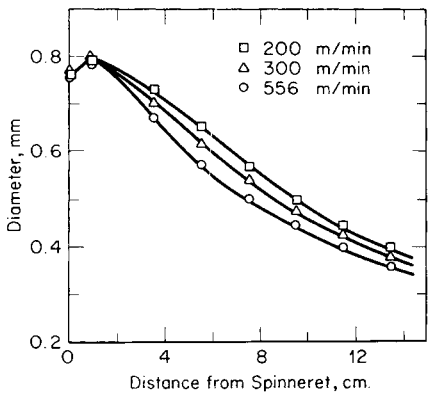

Fig. 11. Diameter profiles for nylon 6 melt for isothermal melt spinning.

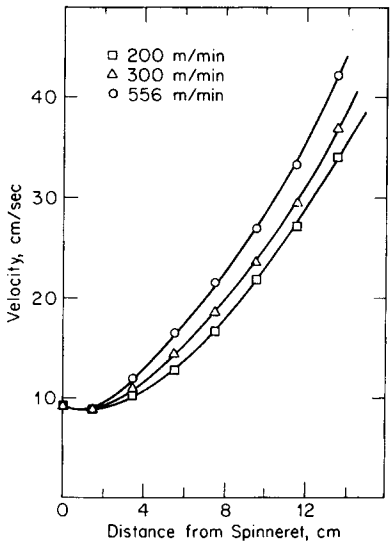

Fig. 12. Velocity as a function of spinline position for isothermal melt spinning.

rather than temperature. This is shown in Figure 13. Further interpretation of these results requires basic rheological data for nylon 6. We will now consider the rheological measurements and then return to the interpretation of the spinning results.

RHEOLOGICAL BEHAVIOR

Results of Measurements

Viscosity. The laminar shear viscosity η ($=\sigma_{12}/\dot{\gamma}$) at 230°, 250°, and 270°C is plotted in Figure 14 as a function of shear rate. The viscosity function is

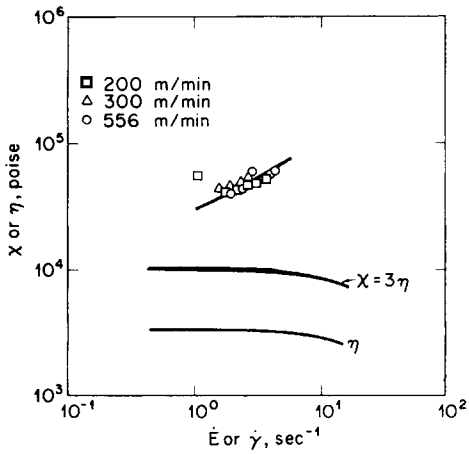

Fig. 13. Elongational viscosity of nylon 6 as determined from isothermal melt-spinning experiments together with the shear viscosity.

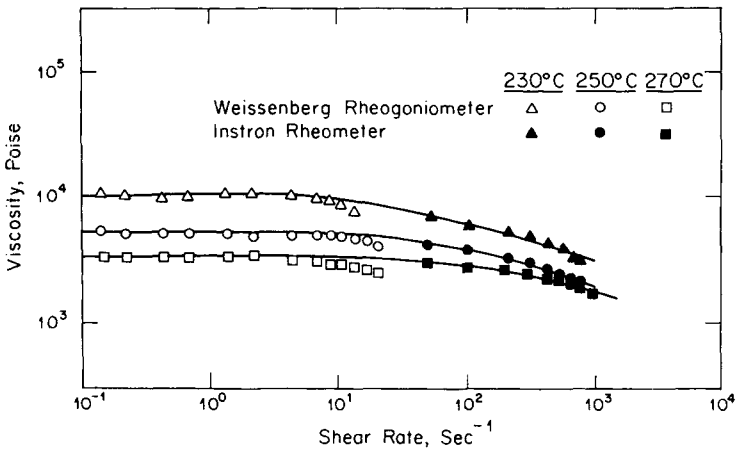

Fig. 14. Viscosity of nylon 6 melt as a function of shear rate at 230°, 250°, and 270°C.

constant at low shear rates and decreases at higher shear rates. At low shear rates, the viscosity at 230°C is of order 10,000 poises; at 250°C, it is about 5000 poises and at 270°C, about 3300 poises.

There was a problem in matching together the capillary rheometer and rheogoniometer viscosity data with the latter data decreasing and taking on smaller values at the shear rates when the data from the two instruments approach. This was believed to be primarily due to the melt emerging from the gap between the cone and the plate in the rheogoniometer. This resulted in a smaller torque and a lower viscosity.

Normal Stresses. The principal normal stress difference coefficient Ψ_1 ($=N_1/\dot{\gamma}^2$) is plotted in Figure 15 as a function of shear rate $\dot{\gamma}$. The data are limited to the range of 4 to 20 sec^{-1}. Unfortunately, in this range of shear rates, the melt emerges from the gap and gives abnormally low viscosity readings.

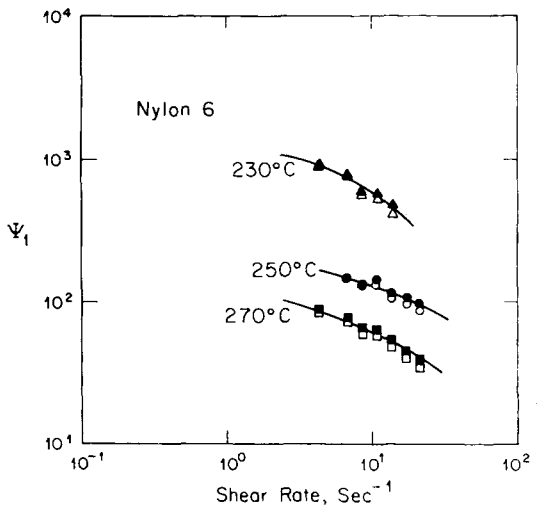

Fig. 15. Principal normal stress difference coefficient Ψ_1 as a function of shear rate $\dot{\gamma}$.

Discussion. The general shape of the viscosity–shear rate function is similar to that of previously reported experimental data[32,34] for nylon 6. In Figure 16, we plot our data together with typical experimental curves of similar nylon 6 melts from the work of Pezzin and Gechele.[32]

Nylon 6 exhibits a much more nearly Newtonian character in these experiments as opposed to polyolefin melts. In Figure 16, we also plot viscosity versus shear rate for a low-density polyethylene (LDPE) melt described in an earlier paper from our laboratories.[49] It can be seen that at low shear rates, the viscosity of the LDPE melt is an order of magnitude higher than that of the nylon 6; but at higher shear rates (200 sec^{-1}), there is a crossover and the LDPE melt has a lower viscosity.

One suspects that the normal stress coefficient data are too low because observations are only possible in the melt-flow instability region where some of the melt from the outer regions of the gap has emerged. If we presume that the gap uniformly is "emptied" of melt through a thickness Δ, we may write eqs. (3) and (5) as follows:

$$\sigma_{12} = \frac{3M}{2\pi(R - \Delta)^3} \tag{12a}$$

$$N_1 = \frac{2F}{\pi(R - \Delta)^2}. \tag{12b}$$

Taking the capillary viscosity data as correct, it may be readily shown that

$$\Psi_1\Big|_{\text{corr}} = \left(\frac{\eta_{\text{cap}}}{\eta_{\text{rheo}}}\right)^{2/3} \Psi_1\Big|_{\text{obs}} \tag{13}$$

i.e., the correct Ψ_1 is greater than the observed Ψ_1 by a factor determined by the corrected viscosity ratio to the $\frac{2}{3}$ power.

In Figure 15, we plot "corrected" $\Psi_1(\dot{\gamma})$ results together with the original data. The value of $\Psi_1(\dot{\gamma})$ is seen to be slightly increased. The procedure outlined above is crude but may effect a correction in the proper direction and perhaps of the proper magnitude.

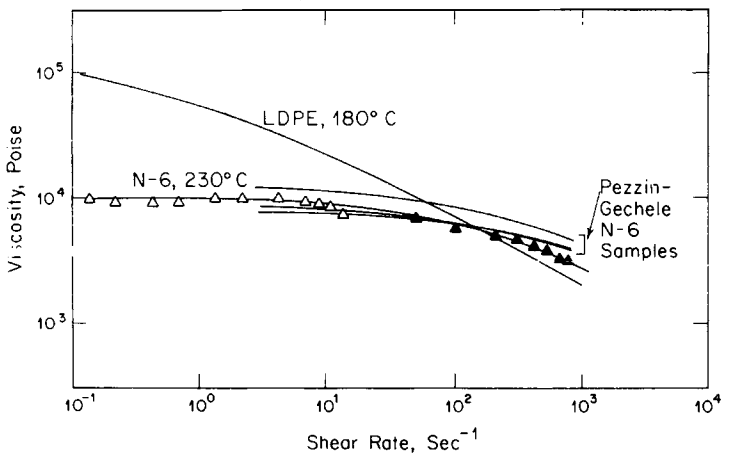

Fig. 16. Comparison of nylon 6 viscosity data with results of Pezzin and Gechele[6] and low-density polyethylene data of Ballenger et al.[45]

We believe one may conclude that the normal stress data and Ψ_1 represent a proper magnitude at the shear rates involved, but one must be wary of the detailed dependence of Ψ_1 on $\dot{\gamma}$ shown in Figure 15.

Another problem that we have not discussed in this section is chemical change. The observation of the polymer in the rheogoniometer turning dark brown or black strongly suggests chemical change. The experimental observations of equal viscosity measurements with increasing or decreasing shear rate and the closeness of viscosity data from the rheogoniometer and capillary rheometer suggest that the influence on the viscosity function at least may be small. However, normal stresses are induced by viscoelastic properties and are more sensitive to the molecular weight distributions. There must be some wariness as to whether the $\Psi_1(\dot{\gamma})$ measured is that of the initial melt.

Interpretation of Viscoelastic Fluid Behavior

The rheological experiments we have cited may be interpreted using the theory of nonlinear viscoelastic fluids.[24,43] First, a "characteristic time" $\bar{\tau}$ of the fluid may be defined from normal stress and shear stress data. This was first shown by Coleman and Markovitz[50] for the "second order fluid" theory, but the same idea remains valid for more sophisticated constitutive equations.[24,28] $\bar{\tau}$ is defined by[50]

$$\bar{\tau} = N_1/2\eta\dot{\gamma}^2. \tag{14}$$

In Figure 17, we plot $\bar{\tau}$ as a function of shear rate. The values of $\bar{\tau}$ are of order 0.025–0.04 sec at 230°C, 0.010–0.015 sec at 250°C, and 0.007–0.011 sec at 270°C.

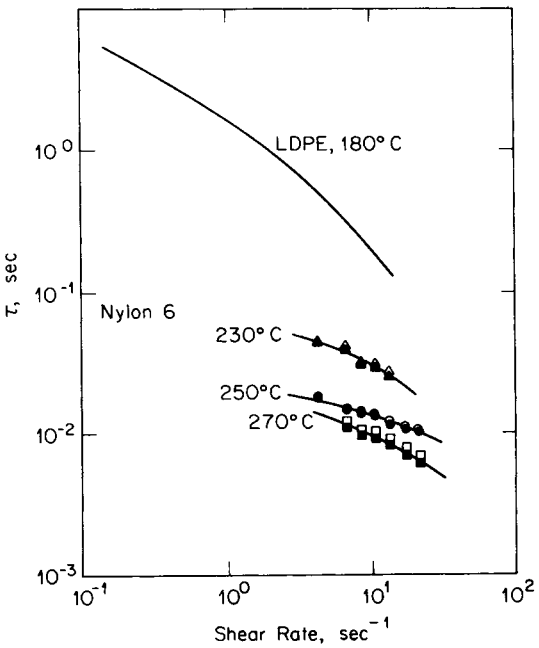

Fig. 17. Plot of $\bar{\tau}$ ($=N_1/2\eta\dot{\gamma}^2$) as a function of shear rate $\dot{\gamma}$ for nylon 6 melt and for a low-density polyethylene of Ballenger et al.[45]

TABLE I
Viscoelastic Parameters for Nylon 6 Determined from Rheological Experiments

Temperature, °C	Linear viscoelastic box distribution		White-Metzner convected Maxwell model		Bogue-White integral model a^b
	H_0, dynes/cm²	τ_m	G, dynes/cm²	$\tau(0)$, sec[a]	
230	1.47×10^5	0.068	2.94×10^5	0.034	0.13
250	1.79×10^5	0.028	3.58×10^5	0.014	0.15(5)
270	1.83×10^5	0.018	3.66×10^5	0.009	0.14

[a] The parameter τ is a function $\tau = \bar{\tau} = n(\Pi_d)/G$.
[b] The other parameters needed are $H(\tau)$, which, for the box distribution, are H_0 and τ_m.

We also plot in Figure 17 $\bar{\tau}$ for a low-density polyethylene melt using the normal stress and viscosity data of Chen (contained in Ballenger et al.[49]). The values of $\bar{\tau}$ are seen to be considerably higher, generally ranging from 0.5 to 5.0 sec.

The value of $\bar{\tau}$ determined using eq. (14) is only an average value of the relaxation time. By definition, we have for the second-order fluid

$$\bar{\tau} = \frac{\int_0^\infty sG(s)\,ds}{\int_0^\infty G(s)\,ds} = \frac{\int_0^\infty \tau H(\tau)\,d\tau}{\int_0^\infty H(\tau)\,d\tau} \tag{15}$$

where $G(t)$ is the relaxation modulus of linear viscoelasticity and $H(\tau)$ is the spectrum of relaxation times. For a Maxwell fluid with a single relaxation time τ, $\bar{\tau}$ is equal to τ. However, if there are several relaxation times, $\bar{\tau}$ will be less than the maximum time τ_m. For example, if we were to apply the box distribution[51]

$$H(\tau) = H_0 \qquad \tau < \tau_m \tag{16}$$

then $\bar{\tau}$ is readily shown to be $\frac{1}{2}\tau_m$. If $H(\tau)$ decreases more slowly at large τ, $\bar{\tau}$ will be an even smaller fraction of τ_m. Studies of $H(\tau)$ and $\bar{\tau}$ for polyolefin melts such as low-density polyethylene by Chen and Bogue[52] suggest that factors of 10 or more may not be unreasonable. However, such melts have much broader molecular weight distributions than nylon 6 and probably much less "box-like" distributions than it. Values of H_0 and τ_m were computed using eqs. (15) and (16) with the low shear rate viscosity η being used to obtain $H_0 \equiv \eta/\tau_m$. The results are given in Table I.

This experimental data may also be fit with the predictions of nonlinear viscoelastic constitutive equations. One widely used constitutive equation is the convected Maxwell-White-Metzner model, which has the form[24,27,53]

$$\sigma = -p\mathbf{I} + \mathbf{P} \tag{17a}$$

$$\frac{\delta \mathbf{P}}{\delta t} = \frac{D\mathbf{P}}{Dt} - \nabla v \cdot \mathbf{P} - P \cdot \nabla \mathbf{v} = 2G\mathbf{d} - \frac{1}{\tau}\mathbf{P} \tag{17b}$$

where $\mathbf{P}$ is the extra-stress tensor; $\mathbf{I}$ is the unit tensor; $\mathbf{v}$ is the velocity vector;

d is the deformation rate tensor; τ is a relaxation time function; and G is a modulus. For laminar shear flow,

$$\eta = G\tau \qquad \Psi_1 = 2G\tau^2 \tag{17c,d}$$

with a zero second normal stress difference. Two rheological quantities, τ and G, arise, with τ being equal to the $\bar{\tau}$ of eq. (8) and Figure 17. Values for G and τ (at low deformation rates) are summarized in Table I.

Generally, the above model is of only qualitative value. We have had more quantitative success in our laboratories correlating rheological data with the Bogue-White model, which has form[24,25,52,54]

$$\sigma = -p\mathbf{I} + \int_0^\infty [m_1(z)\mathbf{c}^{-1} - m_2(z)\mathbf{c}]\, dz \tag{18a}$$

where

$$m_1(z) = \left(1 + \frac{\epsilon}{2}\right)\tilde{m}(z) \qquad m_2(z) = -\frac{\epsilon}{2}\tilde{m}(z) \tag{18b}$$

$$\tilde{m}(z) = \int_{-\infty}^{+\infty} \frac{H\left(\dfrac{\tau'}{1 - a\tau'\overline{\Pi_d}^{1/2}}\right)}{1 - a\tau'\overline{\Pi_d}^{1/2}} \frac{e^{-t/\tau'}}{\tau'}\, d\ln\tau' \tag{18c}$$

where $\Pi_d{}^{1/2}$ is the time-averaged square root of the second invariant Π_d at d. To evaluate η and Ψ_1, one needs to know the spectrum of relaxation times $H(\tau)$. If we accept the box distribution of eq. (16), we then obtain for $\eta(\dot{\gamma})$ and $\Psi_1(\dot{\gamma})$

$$\eta(\dot{\gamma}) = H_0\tau_m \left[\frac{\ln(1 + a\tau_m\dot{\gamma})}{a\tau_m\dot{\gamma}}\right] \tag{19a}$$

$$\Psi_1(\dot{\gamma}) = 2H_0{\tau_m}^2 \left[\frac{\ln(1 + a\tau_m\dot{\gamma})}{(a\tau_m\dot{\gamma})^2} - \frac{1}{a\tau_m\dot{\gamma}(1 + a\tau_m\dot{\gamma})}\right]. \tag{19b}$$

Fitting the experimental data requires knowledge of H_0, τ_m, and a. If we determine τ_m as $2\bar{\tau}$ as follows from the box distribution and H_0 and a from eq. (19a), we obtain the values summarized in Table I.

RHEOLOGICAL INTERPRETATION OF SPINLINE BEHAVIOR

Elongational Viscosity

We shall now try to apply the rheological studies of the previous section. The first point to make is that for a Newtonian fluid, there is a well-established relationship between the shear viscosity η and the elongational viscosity χ. As shown by Trouton,[55] the ratio of these quantities, χ/η, is exactly 3 for incompressible Newtonian fluids. Returning to Figure 13, note the shear viscosity $\eta(\dot{\gamma})$ as a function of $\dot{\gamma}$ and Trouton's[55] prediction of the elongational viscosity as 3η. The experimental χ values are much larger than the predictions obtained using Trouton's relation. The ratio of χ to η is of order 15.

There are no other equivalent studies of χ and η for the same nylon 6 melt in the literature. However, estimates are possible as Pezzin and Gechele[6] have determined the variation of η with molecular weight for this polymer. Using

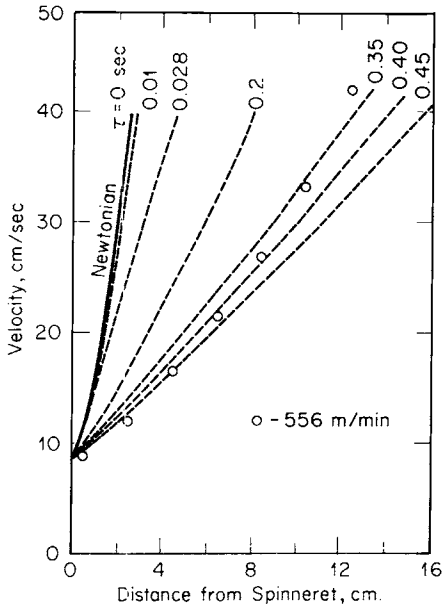

Fig. 18. Experimental and theoretical velocity profiles for nylon 6 melt computed using data of Table I and theory of Denn, Petrie, and Avenas for convected Maxwell model with constant viscosity.

Pezzin and Gechele's data and Hamana, Matsui, and Kato's[17] and Ishibashi, Aoki, and Ishii's[18] nonisothermal $\chi(T)$, we may estimate χ/η. From the data of Hamana et al. for a lower molecular weight polymer, χ/η is of order 8, while from the data of Ishibashi et al. for a high molecular weight polymer, the ratio is 20–40. This would seem to confirm the high values of χ/η that we have observed in our experiments.

The disagreement between χ and the prediction of Trouton is not unexpected, as the nylon 6 is a viscoelastic fluid and similar deviations have been observed for other melts.[20–22] However, the low memory of the nylon 6 makes one wary of this argument.

Viscoelastic Fluid Theory

The question of whether elongational viscosity is an adequate approach to this problem must be discussed. In our runs, the residence time of the melt in the isothermal chamber is of order 0.6 sec, which is very short. If τ_m is $2\bar{\tau}$, then it may be taken from Table I to be about 0.02 sec. This leads to an apparent Deborah number[24,56,57] for the process

$$N_{\mathrm{Deb}} = \tau_m / t_{\mathrm{res}} \tag{20}$$

of 0.03, which is small. However, the value of τ_m may be too small, and the variation in dv/dx along the spinline makes it questionable whether such a choice of t_{res} which gives a global Deborah number is appropriate. Another problem is that the melt which enters the chamber has experienced a severe shearing history in the spinneret. If the melt still remembers this history, an elongational viscosity approach cannot be correct.

TABLE II
Predictions of τ from Denn–Petrie–Avenas Theory and Experimentally Measured Values of τ

Take-up velocity, meters/min	τ Obtained from theory, sec			Experimental $\bar{\tau}$, sec
	Asymptote 1 $\alpha \to 0$	Asymptote 2 $\epsilon/\alpha \to 0$	Numerical solution	
200	0.378	0.694	0.45 to 0.60	
300	0.309	0.520	0.40 to 0.50	≈ 0.01
556	0.245	0.390	0.35 to 0.45	

Of the various treatments of the influence of viscoelasticity on the spinline,[20,25,27,30] only the approach of Denn, Petrie, and Avenas[30] is readily comparable to experiment without exhaustive numerical computation. However, the approach of these authors is essentially based on a convected Maxwell model, eq. (17), which is unable to quantitatively represent viscoelastic response in both the linear and nonlinear range. We have fit Denn et al.'s results to our experimental isothermal data in two manners. First, we used the G and $\tau(0)$ of Table I and computed $v(x)$ and compared it with experiment. This is shown in Figure 18. Generally, it is observed that the experimental velocity data are lower than the predictions from theory. A second approach was to use Denn et al.'s theory as a method of determining τ if G is known. Here we proceeded by using η_0 as the parameter τG. Both the asymptotic solutions as well as the numerical solution were used to compute τ. The results are summarized in Table II.

Generally, the predicted values of τ are about 40 times larger than the experimental ones. The reason for this disagreement is not clear. It is perhaps in some part related to an inability of the rheological model used to represent the behavior of molten nylon 6. However, the discrepancy seems greater than that apparently found by Denn et al. for other melts. Spinneret effects might also need to be considered. Another possibility is that $H(\tau)$ decreases slowly at large τ and that the ratio of $\tau_m/\bar{\tau}$ is large. Also, we might have some error in our $\bar{\tau}$ values determined from rheogoniometer data. We must also be wary of the different degrees of chemical change perhaps occurring in the rheogoniometer and screw extruder.

It is fair to say in concluding this section that the nylon 6 melt responds in the spinline as if it has a much higher elongational viscosity and memory than would be expected based on rheogoniometer shear data.

CONCLUSIONS

1. Nonisothermal melt spinning of nylon 6 melts has been studied over a wide range of take-up velocities. The force components on the threadline with special reference to drag and rheological forces are considered. Rheological response is interpreted in terms of a temperature-dependent elongational viscosity $\chi(T)$.

2. Non-Newtonian viscosity η and normal stresses N_1 have been measured on nylon 6 at 230°, 250°, and 270°C and the data interpreted in terms of the theory of nonlinear viscoelastic flow.

3. Isothermal melt spinning experiments interpreted in terms of elongational

viscosities give χ/η of about 15. This generally agrees with analyses of previously published data on χ and η for separate polymers. Interpretation of the data in terms of the theory of Denn, Petrie, and Avenas for melt spinning of a convected Maxwell fluid shows that agreement is only possible if we use a value of τ 40 times greater than the rheogoniometer value of $\bar{\tau}$.

The authors would like to thank R. L. Ballman, G. E. Hagler, T. A. Hancock, Y. Ide, A. M. Kotliar, J. B. McKoy, M. Matsui, R. Smith, and J. H. Southern for their help in various aspects of this project. They would also like to thank American Enka for supplying the polymer. This research was supported in part by the National Science Foundation under NSF Grant GK 18897.

References

1. W. Sbroli, in *Man-Made Fibers*, Vol. II, H. Mark, S. M. Atlas, and E. Cernia, Eds., Interscience, New York, 1968.
2. W. H. Carothers and G. J. Berchet, *J. Amer. Chem. Soc.*, **52**, 5289 (1930).
3. W. H. Carothers and J. W. Hill, *J. Amer. Chem. Soc.*, **54**, 1566 (1932).
4. W. H. Carothers and J. W. Hill, *J. Amer. Chem. Soc.*, **54**, 1579 (1932).
5. P. Schlack, Germ. Pat. 748,253 (1938); U.S. Pat. 2,241,321 (1941).
6. R. M. Bonner, in *Nylon Plastics* M. I. Kohan, Ed., SPE, Wiley, New York, 1973.
7. A. Ziabicki and K. Kedzierska, *Kolloid-Z.*, **171**, 111 (1960).
8. T. Ishibashi, *J. Appl. Polym. Sci.*, **18**, 2427 (1974).
9. A. Ziabicki and K. Kedzierska, *J. Appl. Polym. Sci.*, **11**, 14 (1959).
10. A. Ziabicki and K. Kedzierska, *Kolloid-Z.*, **171**, 51 (1960).
11. A. Ziabicki, *Kolloid-Z.*, **175**, 14 (1961).
12. A. Ziabicki and K. Kedzierska, *J. Appl. Polym. Sci.*, **6**, 111 (1962).
13. I. Hamana, M. Matsui, and S. Kato, *Melliand Textilber.*, **4**, 382 (1969).
14. I. Hamana, M. Matsui and S. Kato, *Melliand Textilber.*, **5**, 499 (1969).
15. T. Ishibashi, K. Aoki, and T. Ishii, *J. Appl. Polym. Sci.*, **14**, 1597 (1970).
16. T. Kiyotosukuri, H. Hasegawa, and R. Imamura, *Sen-i-Gakkaishi*, **26**, 349, 356, 399 (1970).
17. T. Hancock, J. E. Spruiell, and J. L. White, *J. Appl. Polym. Sci.*, **21**, 1227 (0000).
18. S. Kase and T. Matsuo, *J. Polym. Sci.*, **A3**, 2541 (1965).
19. S. Kase and T. Matsuo, *J. Appl. Polym. Sci.*, **11**, 251 (1967).
20. D. Acierno, J. N. Dalton, J. M. Rodriguez, and J. L. White, *J. Appl. Polym. Sci.*, **15**, 2395 (1971).
21. C. D. Han and R. R. Lamonte, *Trans. Soc. Rheol.*, **16**, 447 (1972).
22. R. R. Lamonte and C. D. Han, *J. Appl. Polym. Sci.*, **16**, 3285 (1972).
23. J. L. White, *J. Appl. Polym. Sci.*, **8**, 2339 (1964).
24. D. C. Bogue and J. L. White, Engineering Analysis of Non-Newtonian Fluids, NATO Agardograph 144, 1970.
25. I. J. Chen, G. E. Hagler, L. E. Abbott, D. C. Bogue, and J. L. White, *Trans. Soc. Rheol.*, **16**, 473 (1972).
26. J. A. Spearot and A. B. Metzner, *Trans. Soc. Rheol.*, **16**, 495 (1972).
27. M. M. Denn, C. J. S. Petrie, and P. J. Avenas, *A.I.Ch.E. J.*, **21**, 791 (1975).
28. J. L. White and J. F. Roman, *J. Appl. Polym. Sci.*, **20**, 1005 (1976).
29. A. Ziabicki, in *Man-Made Fibers*, Vol. 1, H. Mark, S. M. Atlas, and E. Cernia, Eds., Wiley, New York, 1967.
30. J. L. White and Y. Ide, in *Fiber and Yarn Processing*, J. L. White, Ed., *Appl. Polym. Symp.*, **27**, 61 (1975).
31. J. R. Schaefgen and P. J. Flory, *J. Amer. Chem. Soc.*, **70**, 2709 (1948).
32. G. Pezzin and G. B. Gechele, *J. Appl. Polym. Sci.*, **8**, 2195 (1964).
33. M. I. Kohan, in *Nylon Plastics*, M. I. Kohan, Ed., SPE, Wiley, New York, 1973.
34. A. M. Kotliar, unpublished research, 1975.
35. V. Bankar, J. E. Spruiell, and J. L. White, *J. Appl. Polym. Sci.*, to appear.
36. L. E. Abbott and J. L. White, *Appl. Polym. Symp.*, **20**, 247 (1973).
37. J. R. Dees and J. E. Spruiell, *J. Appl. Polym. Sci.*, **18**, 1053 (1974).

38. J. L. White, K. C. Dharod, and E. S. Clark, *J. Appl. Polym. Sci.*, **18,** 2539 (1974).
39. J. E. Spruiell and J. L. White, *Polym. Eng. Sci.*, **15,** 660 (1975).
40. J. E. Spruiell and J. L. White, in *Fiber and Yarn Processing*, J. L. White, Ed., *Appl. Polym. Symp.*, **27,** 121 (1975).
41. Y. Ide and J. L. White, *J. Appl. Polym. Sci.*, **20,** 2511 (1976).
42. R. Eisenschitz, B. Rabinowitsch, and K. Weissenberg, *Mitt. Deut. Materialprüfungsanhalten,* **Sund IX,** 91 (1929).
43. S. Middleman, *The Flow of High Polymers,* Wiley, New York, 1968.
44. S. M. Freeman and K. Weissenberg, *Nature,* **161,** 324 (1948).
45. M. Inoue, *J. Polym. Sci. A,* **1,** 2013 (1963).
46. B. C. Sakiadis, *A.I.Ch.E. J.*, **7,** 467 (1961).
47. Y. Sano and K. Orii, *Sen-i-Gakkaishi,* **24,** 212 (1968).
48. M. Matsui, *Trans. Soc. Rheol.*, **20,** 465 (1976).
49. T. F. Ballenger, I. J. Chen, G. E. Hagler, D. C. Bogue, and J. L. White, *Trans. Soc. Rheol.*, **15,** 195 (1971).
50. B. D. Coleman and H. Markovitz, *J. Appl. Phys.*, **35,** 1 (1964).
51. A. V. Tobolsky, *Properties and Structure of Polymers,* Wiley, New York, 1960.
52. I. J. Chen and D. C. Bogue, *Trans. Soc. Rheol.*, **16,** 59 (1972).
53. J. L. White and A. B. Metzner, *J. Appl. Polym. Sci.*, **8,** 1367 (1963).
54. T. Takaki and D. C. Bogue, *J. Appl. Polym. Sci.*, **19,** 419 (1975).
55. F. T. Trouton, *Proc. R. Soc.*, **A77,** 426 (1906).
56. M. Reiner, *Physics Today,* 62 (January 1964).
57. A. B. Metzner, J. L. White, and M. M. Denn, *A.I.Ch.E. J.*, **12,** 863 (1966); *Chem. Eng. Progr.*, **62**(12), 81 (1966).

Received April 23, 1976
Revised June 24, 1976